Proceedings of the 12th International Conference on Low Energy Antiproton Physics (LEAP2016)
Downloaded from journals.jps.jp by 128.141.46.242 on 03/23/18

Proc. 12th Int. Conf. Low Energy Antiproton Physics (LEAP2016)
JPS Conf. Proc. **18**, 011019 (2017)
https://doi.org/10.7566/JPSCP.18.011019

A Test of Charge-Parity-Time Invariance at the Atto-Electronvolt Scale

Andreas Mooser[1], Takashi Higuchi[1,2], Christian Smorra[1,3], Hiroki Nagahama[1,2], Nathan Leefer[4], Georg Schneider[1,5], Stefan Sellner[1], Klaus Blaum[6], Yasuyuki Matsuda[2], Wolfgang Quint[7], Jochen Walz[4,5], Yasunori Yamazaki[8] and Stefan Ulmer[1]

[1]*Ulmer Initiative Research Unit, RIKEN, 2-1 Hirosawa, Wako, Saitama 351-0198, Japan*
[2]*Graduate School of Arts and Science, University of Tokyo, 3-8-1 Komaba, Meguro-ku, Tokyo 153-8902, Japan*
[3]*CERN, CH-1211 Geneva 23, Switzerland*
[4]*Helmholz-Institut Mainz, Johann-Joachim-Becher-Weg 36, 55128 Mainz, Germany*
[5]*Institut für Physik, Johannes Gutenberg-Universitt Mainz, Staudingerweg 7, 55128 Mainz, Germany*
[6]*Max-Planck-Institut für Kernphysik, Saupfercheckweg 1, 69117 Heidelberg, Germany*
[7]*Atomphysik, GSI-Helmholzzentrum für Schwerionenforschung, Planckstraße 1, 64291 Darmstadt, Germany*
[8]*Atomic Physics Laboratory, RIKEN, 2-1 Hirosawa, Wako, Saitama 351-0198, Japan*

E-mail: andreas.mooser@cern.ch

(Received May 30, 2016)

We developed a novel fast measurement procedure for cyclotron frequency comparisons of two individual particles in a Penning trap, which enabled us to compare the charge-to-mass ratio of the proton and the antiproton with a fractional precision of 69 parts per trillion. To date this is the most precise test of charge-parity-time invariance using baryons. Our measurements were performed at cyclotron frequencies of about 30 MHz, which means that charge-parity-time symmetry holds at the atto-electronvolt scale.

KEYWORDS: Antiproton, Proton, Magnetic moment, Charge-to-mass ratio, CPT invariance, Penning trap

1. Introduction

Invariance under the combined transformation of charge, parity and time is a fundamental symmetry of all local, Lorentz-invariant quantum field theories combined in the Standard Model of particle physics [1]. The general validity of this invariance is an open question. This triggers a variety of different experiments, which aim at tests of CPT invariance by comparing the properties of matter and antimatter with highest precision [2–4]. Among those is the *Baryon Antibaryon Symmetry Experiment* (BASE), which tests CPT symmetry by comparing the magnetic moments and the charge-to-mass ratios of single protons and antiprotons in an advanced Penning-trap system [5].
Up to now the most precise value for the comparison of the proton and the antiproton charge-to-mass ratios resulted from measurements performed by the TRAP collaboration in the 1990s [6]. Here a relative precision of 90 parts per trillion has been achieved. Very recently we improved this measurement to a fractional precision of 69 parts per trillion [7].In this article we discuss our measurements and give an outlook towards a further improved comparison of the charge-to-mass ratios.

©2017 The Author(s)

This article is available under the terms of the Creative Commons Attribution 4.0 License. Any further distribution of this work must maintain attribution to the author(s) and the title of the article, journal citation, and DOI.

Proceedings of the 12th International Conference on Low Energy Antiproton Physics (LEAP2016)
Downloaded from journals.jps.jp by 128.141.46.242 on 03/23/18

2. Experimental Setup

To perform such high-precision comparisons of the fundamental properties of protons and antiprotons, BASE operates an advanced Penning-trap setup at the antiproton decelerator (AD) at CERN, Switzerland. Each Penning trap consists of five gold-plated oxygen-free-electrolytic copper electrodes in cylindrical design with inner diameters of 9 mm [8]. The Penning traps are in compensated and orthogonal design [9] and are placed in the horizontal bore of a superconducting magnet at $B_0 = 1.964\,\mathrm{T}$, see Fig. 1. High-precision voltage sources (UM 1-15LN, Stahl Electronics Mettenheim) produce the electric trapping potential. In total, BASE operates four individual Penning traps in a stacked configuration. The reservoir trap and the precision trap allow for precise and accurate frequency measurements on single ions within the homogeneous center of the superconducting magnet. In addition one of these traps is used for the storage of a cloud of particles and serves as a source of antiprotons for months during accelerator shutdown [10]. Two additional Penning traps, which are placed at the downstream side (not shown in Fig. 1), are superimposed with an inhomogeneous magnetic field. This allows for real-time monitoring of the particle's energy [5] and the analysis of the spin state [11,12], which is important for a measurement of the magnetic moment. The individual Penning traps are connected by transport electrodes which allow for adiabatic shuttling of the particles between the traps. The entire electrode stack is mounted in an indium sealed cylindrical trap chamber with a volume of about 1.2 l and cooled down to liquid helium temperature. This allows to reach ultra-low pressures of 10^{-17} mbar and particle storage times of several years.

The trajectory of a charged particle in a Penning trap can be described by the superposition of three

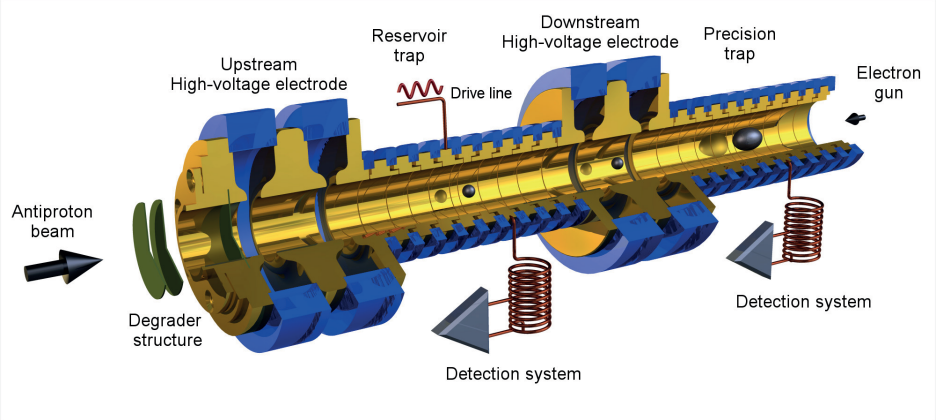

Fig. 1. Schematic of the advanced Penning-trap system at BASE. For details see text.

independent harmonic oscillator motions, the axial motion along the magnetic field lines with frequency $\nu_z \approx 700\,\mathrm{kHz}$, and two radial motions: the magnetron motion with frequency $\nu_- \approx 7\,\mathrm{kHz}$ and the modified cyclotron motion with frequency $\nu_+ \approx 30\,\mathrm{MHz}$. The free cyclotron frequency is obtained by applying the invariance theorem $\nu_c^2 = \nu_+^2 + \nu_z^2 + \nu_-^2$ [13]. To measure the oscillation frequency of the particle's eigenmotions, the non-destructive image current detection method is used [14]. Thus each Penning trap is provided with dedicated detection systems, consisting of a high-quality superconducting coil and a low noise small-signal amplifier [15].

Antiprotons provided by the AD are decelerated using a degrader structure, mounted on the upstream side of the electrode stack, and subsequently captured in the trap applying triggered high voltage on the high-voltage electrode, see Fig. 1. In addition, the antiproton bunches produce negatively charged hydrogen atoms H^- from hydrogen gas frozen out on the degrader structure either by asymmetric

Proceedings of the 12th International Conference on Low Energy Antiproton Physics (LEAP2016)
Downloaded from journals.jps.jp by 128.141.46.242 on 03/23/18

dissociation of molecular hydrogen or by electron capture of atomic hydrogen. Afterward electron cooling is applied to reduce the energies of both ion species to μeV-energies. To prepare a clean composite cloud of antiprotons and H^- ions, subsequently axial drives are applied for cleaning of contaminants and the electrons. Figure 2 shows a spectrum of the detector after the preparation, signal peaks induced by trapped antiprotons and negatively charged hydrogen ions are visible besides the noise resonance of the detector.

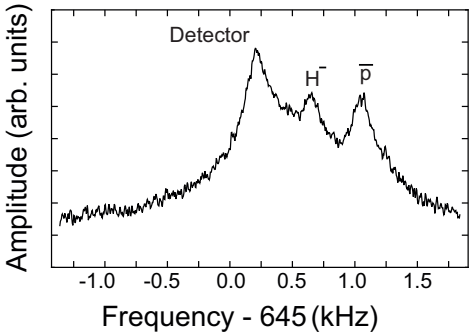

Fig. 2. Fast Fourier Transform (FFT) signal of one of the axial detection systems after the initial preparation of a clean composite cloud of antiprotons and negative hydrogen ions H^- ions from Ref. [5]. Besides a broad resonance caused by the Johnson-Nyquist noise of the detector two individual signals can be seen. These signals are due to the image currents induced by a cloud of antiprotons and H^- ions, respectively.

3. Operation of the reservoir trap

Besides being usable as a precision measurement trap the reservoir trap allows the storage of a cloud of antiprotons and serves as a source of antiprotons during accelerator shutdown when external magnetic field fluctuations are low. To this end, we developed a novel separation and merging method using adiabatic potential ramps, which enables an extraction of an arbitrary number of particles, e.g. a single one, into the measurement traps [10]. In a first step the particle cloud is centered with respect to the central ring electrode of the reservoir trap and a trapping voltage of 13.5 V is applied. Next a potential offset ΔU is applied to one of the correction electrodes adjacent to the central ring electrode. This introduces an additional electric field of $\Delta E = 0.32\,\mathrm{V/m}\cdot\Delta U/V$, which shifts the center of mass motion with respect to the central ring electrode. In order to separate the cloud in a next step, the voltage applied to the central ring electrode is ramped down from 13.5 V to −13.5 V. In the last step one of the individual ion clouds is transported to and stored in the downstream high voltage electrode, and the trap content is analyzed. Applying the method described in [14], the number of the particles in the two individual clouds can be counted in the reservoir trap. Figure 3 shows the fraction of particles extracted to the individual particle clouds as a function of the center of mass position of the cloud. The method allows a reliable extraction of fractions of particles ranging down to a single one. In addition, reversing the order of the applied separation sequence the individual particle clouds were merged. In Fig. 3 the blue data points give the fraction of particles counted afterwards. The results show that within our measurement uncertainties the complete sequence, including separation and merging, is loss free.

Proceedings of the 12th International Conference on Low Energy Antiproton Physics (LEAP2016)
Downloaded from journals.jps.jp by 128.141.46.242 on 03/23/18

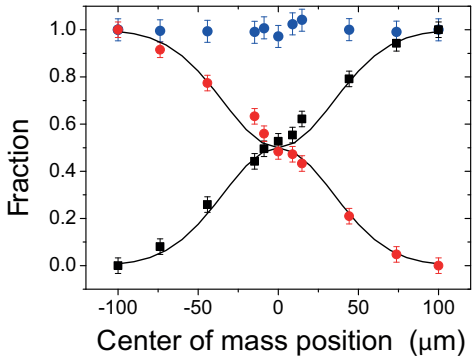

Fig. 3. Fractions of extracted particles compared to the initial number of particles as a function of the center-of-mass position of the ion clouds with respect to the central ring electrode from Ref. [10]. Black data points show the fraction extracted to the downstream side of the apparatus. Likewise red data points show the fraction extracted to the upstream side of the apparatus. Blue data points show the fraction of particles after the two separated particle clouds have been merged again. The solid lines are theoretical calculations. For further details see text.

4. High-precision comparison of the proton to antiproton charge-to-mass ratio

After preparation of a clean composite cloud of antiprotons and H^- ions in the precision trap, we apply our separation technique to load a single antiproton into the reservoir trap and a single H^- ion in the upstream high-voltage electrode. The H^- ion is used instead of a proton which avoids systematic shifts caused by polarity switching of trapping voltages. The mass of the H^- ion is given by

$$m_{H^-} = m_p + 2m_e - E_b - E_a. \tag{1}$$

Here m_e is the mass of the electron [16], m_p is the mass of the proton [17], E_b is the binding energy of the first electron [18] and E_a the electron affinity being the binding energy of the second electron [19]. In addition, the motional electric field E_m experienced by the H^- ion in its instantaneous rest frame induces a dipole moment $d_{ind} = \alpha_{pol,H^-} E_m$, which adiabatically follows the motional electric field. Here α_{pol,H^-} is the polarizability of the H^- ion. This generates an additional Lorentz force, which alters the cyclotron frequency and can be accounted for by an effective mass increase of $\alpha_{pol,H^-} B_0^2$ [20]. If CPT invariance holds, the expected cyclotron frequency ratio is

$$R_{th} = \frac{(\nu_c)_{\bar{p}}}{(\nu_c)_{H^-}} = \frac{(q/m)_{\bar{p}}}{(q/M)_{H^-}} \frac{B_0/2\pi}{B_0/2\pi} = \frac{(q/m)_{\bar{p}}}{(q/M)_{H^-}} = 1.0010892187536(1), \tag{2}$$

the precision limited by the accuracy of the proton mass in the electron-to-proton mass ratio, see Tab. I. In an ideal measurement the magnetic field strength B_0 is assumed to be equal and cancel out in the frequency ratio. Since actual measurements of R are carried out by sequentially measuring the cyclotron frequencies, we investigated the temporal fluctuations of the magnetic field by a series of cyclotron frequency measurements.

In case the measurement of the cyclotron frequency not triggered with respect to the antiproton deceleration cycle, the Allan deviation of the cyclotron frequency shows an oscillating component caused by a beat with a period of 21 min between magnet ramps during the antiproton deceleration cycle and our cyclotron frequency measurement can be observed, see Fig. 4a). If the measurement is triggered with respect to the antiproton injection trigger and the duration of the cyclotron frequency measurements is matched to the antiproton deceleration cycle, this beat vanishes and only white noise with a standard deviation of 160 mHz and a random walk component with 220 mHz contribute. Repeating the same measurement during a decelerator shutdown did not affect the white noise contribution while

Proceedings of the 12th International Conference on Low Energy Antiproton Physics (LEAP2016)
Downloaded from journals.jps.jp by 128.141.46.242 on 03/23/18

Table I. Dimensionless contributions and uncertainties to the theoretical charge-to-mass ratio.

	contribution (10^{-12})	uncertainty (10^{-12})
$2m_e/m_p$	1089234042.7	0.1
E_b/m_p	-14493.0	$< 10^{-3}$
E_a/m_p	-803.8	$< 10^{-5}$
$\alpha_{pol,H^-} B_0^2/m_p$	7.7	$< 10^{-3}$
$\sum$	1089218753.6	0.1

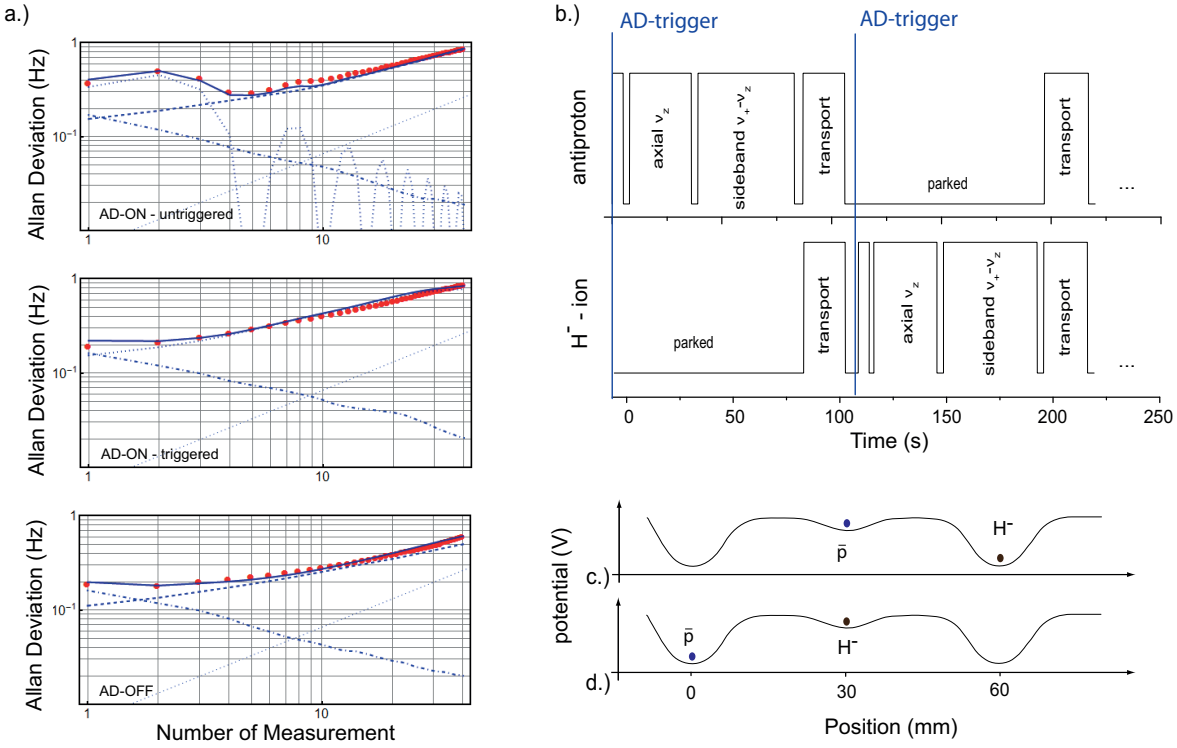

Fig. 4. Allan deviation of subsequent cyclotron frequency measurements and schematic of the measurement sequence for the high-precision comparison of the proton to antiproton charge-to-mass ratio from Ref. [5]. In a) Allan deviations of cyclotron frequency measurements of a single antiproton under different conditions are shown. A white noise, a random walk and an oscillating contribution are shown as dashed-dotted, dashed and dotted line, respectively. In b) the timing sequence of the measurement is shown. In c) and d) the potential configurations during the measurement of the antiproton and H^- ion cyclotron frequencies are shown.

the random walk is further reduced to 160 mHz, which indicates the presence of additional magnetic field fluctuations caused by the accelerator during operation.

Based on the latter results, each measurement cycle of the charge-to-mass ratio comparison is triggered by the antiproton injection into CERN's antiproton decelerator. One cycle starts with cooling of the magnetron motion of the antiproton by applying a quadrupole drive at the respective magnetron axial sideband frequency $\nu_z + \nu_-$, which couples the magnetron motion to the axial motion. Afterward, the free cyclotron frequency of the antiproton is measured at the potential configuration shown in Fig. 4c). To this end the axial frequency of the antiproton $\nu_{z,\bar{p}}$ and the reduced cyclotron frequency $\nu_{+,\bar{p}}$ as described in [24] is measured. The magnetron frequency is determined by $\nu_{-,\bar{p}} \cong \nu_{z,\bar{p}}^2/\nu_{+,\bar{p}}$ being a sufficient approximation at the current level of precision. Finally, the free cyclotron frequency

Proceedings of the 12th International Conference on Low Energy Antiproton Physics (LEAP2016)
Downloaded from journals.jps.jp by 128.141.46.242 on 03/23/18

of the antiproton is obtained by using the relation $\nu_c^2 = \nu_+^2 + \nu_z^2 + \nu_-^2$. After a simultaneous adiabatic transport of the antiproton to the downstream high-voltage electrode and the H^- ion to the reservoir trap, the potential configuration as shown in Fig. 4d) is applied. Subsequently the magnetron motion of the H^- ion is cooled and its free cyclotron frequency is measured in the same way as described for the antiproton. Note that the potential configurations during both cyclotron frequency measurements are equal except for a small difference in the ring voltage, which reduces systematic effects caused by particle shifts due to unequal potential configurations within a residual magnetic inhomogeneity of $B_1 = 7.58(42)\,\mathrm{mT\,m^{-1}}$. Hence a single cyclotron frequency comparison takes exactly two antiproton deceleration cycles, which is about 200 s. This is about 50 times faster than in previous measurements [6] and thus less sensitive to external systematic drifts. Moreover, it allows us to accumulate much higher statistics than achieved before.

Figure 5 shows the experimental results. In total we performed 6521 cyclotron frequency compar-

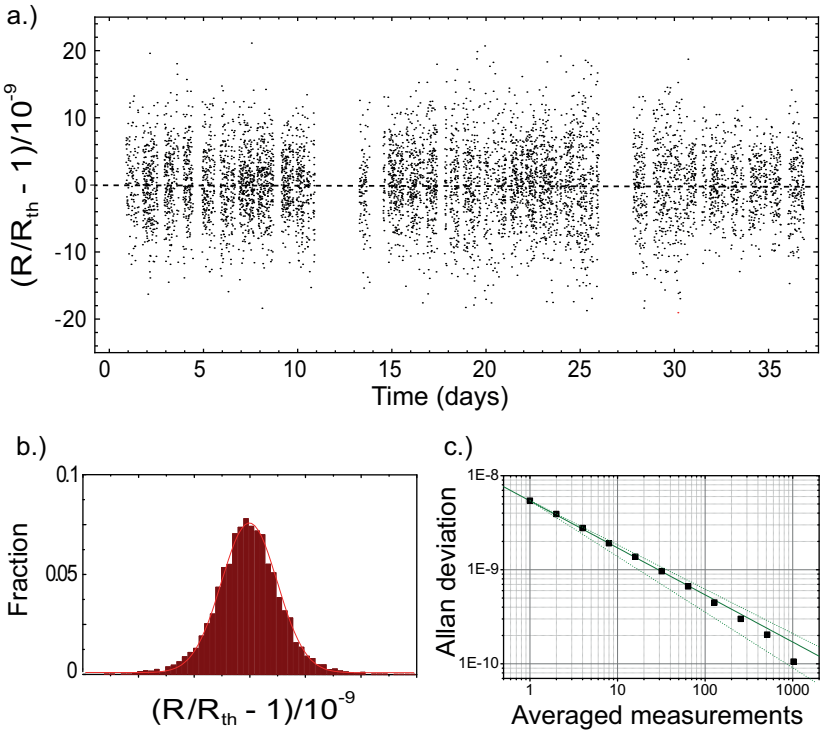

Fig. 5. Results on the comparison of the proton to antiproton charge-to-mass ratio from Ref. [7]. a) About 6521 cyclotron frequency comparisons have been recorded over a time period of about one month. In b) a projected histogram of the measured cyclotron frequency ratios are shown. From a Maximum-Likelihood fit using a normal distribution as line-shape we extract the ratio with a statistical uncertainty of 64 ppt. In c) the Allan deviation of the measured ratios with a fit to the data with slope −0.501(1) is shown. This confirms that the ratio fluctuations follow a Gaussian white noise distribution.

isons over a time period of about one month. From a Maximum-Likelihood estimate using a normal distribution as line-shape model we extract an experimental value for the dimensionless ratio of charge-to-mass ratios of

$$R = 1.001089218872(64). \tag{3}$$

The usage of a normal distribution is supported by the evaluation of the Allan deviation, see Fig. 5 c). To further verify our data analysis we also evaluated the cyclotron frequency ratios of $\bar{p}$-$\bar{p}$ and H^--H^-

Proceedings of the 12th International Conference on Low Energy Antiproton Physics (LEAP2016)
Downloaded from journals.jps.jp by 128.141.46.242 on 03/23/18

in subsequent cycles. From these we extract $1 - 1/R = -3(79)$ ppt, which further justifies our data analysis and shows that systematic magnetic field drifts are not present.
The dominant systematic shift is related to a mV-detuning of the trapping voltages, which is required to tune the axial oscillation frequency of the antiproton as well as the hydrogen ion into resonance with the axial detection system. In presence of different contact potentials, offset potentials and machining imperfections the change in ring voltage leads to a shift of the equilibrium position of the antiproton with respect to the equilibrium position of the H^- ion. In presence of a magnetic field gradient $B_1 = 7.58(42)\,\mathrm{mT\,m^{-1}}$, both cyclotron frequencies are measured at slightly different magnetic fields. In total the experimental result has to be corrected by $-117(26)$ ppt, which gives the final result

$$R = 1.001089218755(64)(26). \tag{4}$$

Here the first value in parentheses gives the statistical uncertainty and the second value in parentheses the systematic uncertainty. Our final result is within error bars in agreement with the theoretical prediction. From this we conclude that in this case CPT is conserved. Since our measurements probe the kinetic energy of the cyclotron mode $E_c = \hbar\omega_c \approx$ μeV with a relative precision of 10^{-12} our measurements are sensitive at an absolute energy scale of 10^{-18}eV.

5. Outlook

To overcome the previous limitations two improvements have meanwhile been implemented. First, a new superconducting magnet has been installed. This allows for a precise shimming of the residual magnetic field inhomogeneity by more than one order of magnitude, which means that the associated systematic uncertainty of 26 ppt will be reduced by a factor of at least 10. Second, we implemented a so-called self-shielding coil, which significantly reduces external magnetic field fluctuations in the center of our Penning trap [21]. Hence, in the new setup we reduced the cyclotron frequency fluctuations by a factor of four, see Fig. 6. Under the same experimental conditions this also reduces the statistical uncertainty by the same factor. In combination the first measurements with the improved setup suggest that in future an improved charge-to-mass ratio comparison at the level of 20 ppt is feasible.
Even higher precision can be reached by simultaneous storage of both ions in the same Penning trap

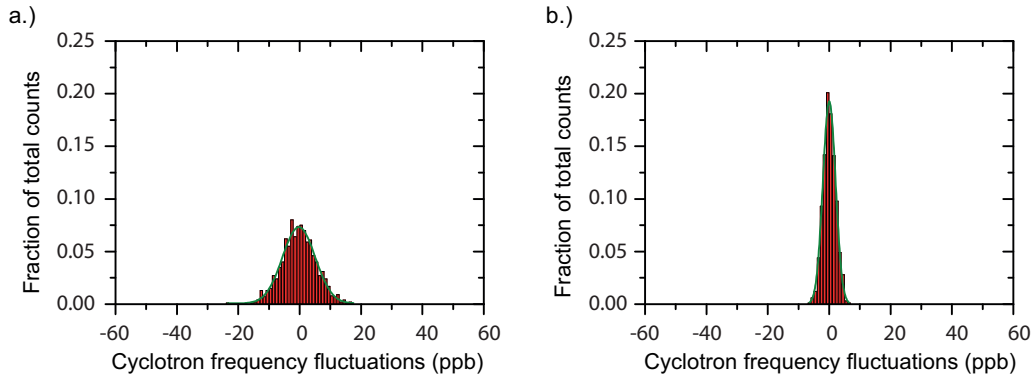

Fig. 6. Cyclotron frequency fluctuations. In a) the cyclotron frequency fluctuations observed with the apparatus used for the high-precision comparison of the antiproton-to-proton charge-to-mass ratio are shown. In b) these fluctuations could be reduced by a factor 4 after installing a new superconducting magnet which allows for a precise shimming of residual magnetic field inhomogeneities, and the installation of a self-shielding coil.

Proceedings of the 12th International Conference on Low Energy Antiproton Physics (LEAP2016)
Downloaded from journals.jps.jp by 128.141.46.242 on 03/23/18

and applying phase-sensitive detection methods as demonstrated in [20, 22]. Here the storage of both ions at the same orbit in the same Penning trap allows to balance out many sources of noise and error, for example magnetic field fluctuations, which might become relevant at higher precisions. Applying these methods to charge-to-mass comparisons of the proton and the antiproton relative precisions of 10 ppt or better are possible.
Up to now the test of CPT invariance by comparison of the magnetic moments of the proton and the antiproton is limited by the knowledge of the antiproton magnetic moment. Using a single Penning trap method, the antiproton magnetic moment has been measured to a relative precision of 4.4 parts per million [4]. BASE aims at an improved comparison by three orders of magnitude by applying the double Penning-trap method [23], which we successfully implemented to measure the proton magnetic moment with a fractional precision of 3.3 parts per billion [24].

6. Conclusion

By comparing the cyclotron frequencies of an antiproton to an H^- ion with a relative precision of 69 ppt we performed the most precise test of CPT invariance in the baryonic sector so far. The measurements were performed at cyclotron frequencies of about 30 MHz, which means that in this case CPT violating contributions to the Standard Model of particle physics can be excluded at the atto-electronvolt scale. Further upgrades of the apparatus suggest that an improved comparison by a factor of four is possible.

7. Acknowledgment

We acknowledge support by the Antiproton Decelerator group and all other CERN groups which provide support to Antiproton Decelerator experiments. We acknowledge financial support by the RIKEN Initiative Research Unit Program, RIKEN President Funding, RIKEN Pioneering Project Funding, RIKEN FPR Funding, the RIKEN JRA Program, the Grant-in-Aid for Specially Promoted Research (grant number 24000008) of MEXT, the Max-Planck Society, the EU (ERC advanced grant number 290870-MEFUCO), the BMBF, the Helmholtz-Gemeinschaft, and the CERN Fellowship programme.

References

[1] G. Lueders, Ann. Phys. **2**, 1 (1957).
[2] C. Amole *et al.*, Nature **483**, 439 (2012).
[3] N. Kuroda *et al.*, Nat. Comm. **5**, 3089 (2014).
[4] J. DiSciacca *et al.*, Phys. Rev. Lett. **110**, 130801 (2013).
[5] C. Smorra *et al.*, Eur. Phys. J. ST **224**, 14 (2015).
[6] G. Gabrielse *et al.*, Phys. Rev. Lett. **82**, 3198 (1999).
[7] S. Ulmer *et al.*, Nature **524**, 196 (2015).
[8] G. Gabrielse *et al.*, Appl. Phys. Lett. **55**, 2144 (1989).
[9] L.S. Brown and G. Gabrielse, Rev. Mod. Phys. **58**, 233 (1986).
[10] C. Smorra *et al.*, Int. J. Mass spectrom. **385**, 10 (2015).
[11] H. Dehmelt *et al.*, Proc. Natl. Acad. Sci. **83**, 2291 (1986).
[12] W. Quint, *et al.*, Nucl. Instr. Meth. B **214**, 207 (2004).
[13] L.S. Brown and G. Gabrielse, Phys. Rev. A **25**, 2423 (1982).
[14] D.J. Wineland and H.G. Dehmelt, J. Appl. Phys. **46**, 919 (1975).
[15] A. Mooser *et al.*, Can. J. Phys **89**, 165 (2011).
[16] S. Sturm *et al.*, Nature **506**, 467 (2014).
[17] R.S. Van Dyck Jr *et al.* AIP Conf. Proc. **457**, 101 (1999).
[18] C. G. Parthey *et al.*, Phys. Rev. Lett. **107**, 203001 (2011).
[19] A.K. Bhatia and R.J. Drachmann, J. Phys. At. Mol. Opt. Phys. **27**, 1299 (1994).

Proceedings of the 12th International Conference on Low Energy Antiproton Physics (LEAP2016)
Downloaded from journals.jps.jp by 128.141.46.242 on 03/23/18

[20] J. K. Thompson *et al.*, Nature **430**, 58 (2004).
[21] G. Gabrielse and J. Tan, J. Appl. Phys. **63**, 5143 (1988).
[22] S. Rainville *et al.*, Science **303**, 334 (2004).
[23] A. Mooser *et al.*, Phys. Lett. B **723**, 78 (2013).
[24] A. Mooser *et al.*, Nature **509**, 596 (2014).